SF2A 2012
S. Boissier, P. de Laverny, N. Nardetto, R. Samadi, D. Valls-Gabaud and H. Wozniak (eds)

SCIROCCO: SIMULATION CODE OF INTERFEROMETRIC-OBSERVATIONS FOR ROTATORS AND CIRCUMSTELLAR OBJECTS

M. Hadjara[1, 2], F. Vakili [2], A. Domiciano de Souza [2], F. Millour [2] and P. Bendjoya[2]

Abstract. The VLTI (Very Large Telescope Interferometer) makes available milli-arcsecond-scale observations in the infrared. It offers new possibilities for constraining stellar structures such as polar jets, equatorial disks and rotationally-flattened photospheres of Be stars. Such constraints allows us to better estimate the stellar fundamental parameters and refine the mechanisms such as mass loss, pulsation and magnetism that govern the variability and evolution of these stars.

In this paper we present a chromatic semi-analytical model of fast rotators, which allows us to study the dynamics and the interaction between the photosphere and the wind of fast rotating stars of A, B and F spectral types. Our simple analytical model addresses the oblateness, inclination and position angle of the rotation axis of the star. It produces iso-velocity maps and intensity maps. It includes line profiles, limb-darkening and the von Zeipel effect.

SCIROCCO: **S**imulation **C**ode of **I**nterferometric-observations for **RO**tators and **C**ir**C**umstellar **O**bjects, includes all the parameters cited above in order to be a fast, powerful and light simulation tool for interpreting high angular resolution observations of rotating stars.

Keywords: Stars: rotation, Methods: numerical, Techniques: interferometric, Techniques: high angular resolution

1 Introduction

The stars with low metallicity are supposed to produce little or no magnetic field. This absence of magnetic field leads to a high spin-up during the contraction then formation of these stars (Martayan et al. 2006). This rotation rate can attain more than 80% of the critical, or breakup, velocity $v_c = \sqrt{(GM/R_c)}$ (with R_c the equatorial radius at this velocity) in some cases. These fast-rotating stars are called "fast rotators" and exhibit a number of peculiar characteristics (Domiciano de Souza et al. 2003), among which geometrical flattening, coupled with gravitational darkening von Zeipel (1924), making the poles hotter than the equator.

The models from Collins & Sonneborn (1977) indicate a two-components spectral energy distribution (SED) for these stars, with an infrared excess due to gravity darkening. Hence, it is not easy to place these stars in one single spectral classification, as the observed SED depends on its rotational velocity and inclination angle (Maeder & Peytremann 1972).

Furthermore, rapid rotation induce an additional change in the apparent spectral type and class of the star (Collins & Harrington 1966). Indeed, the full widths at half-maximum (FWHM) of UV lines are generally narrower (up 0.2 km/s) than those of the visible lines due again to gravitational darkening (Hutchings et al. 1979), since the spectral lines, depending on the temperature and gravity, are not formed uniformly on the star. This has an impact on the estimate of the inclination angle (Hutchings & Stoeckley 1977) and, hence, the estimation of the spectral type of the star. A classification based on the spectral ratio between the widths of these lines would be distorted by this effect (Collins 1974).

In addition, mechanisms such as meridional circulation and/or turbulence may affect the internal structure of the star and its evolution (Meynet 2009). Thus, fast rotators have always been considered as a physics laboratory to study stellar interiors, stellar evolution and primordial stars.

[1] Centre de Recherche en Astronomie, Astrophysique et Géophysique (CRAAG) Route de l'Observatoire, B.P. 63, Bouzareah, 16340, Alger, Algérie.; m.hadjara@craag.dz

[2] Laboratoire J.-L. Lagrange UMR 7293- Observatoire de la Côte d'Azur (OCA), Université de Nice-Sophia Antipolis (UNS), Centre National de la Recherche Scientifique (CNRS), Campus Valrose, 06108 Nice cedex 2, France.; Massinissa.Hadjara@oca.eu

In this context, spectrally-resolved long baseline interferometry offers new opportunities to observe the details of such stars with enough spatial resolution (van Belle 2012). We describe in this paper a numerical model that includes a subset of the different mechanisms described above: fast rotation, gravity darkening, and stellar pulsations. It produces intensity maps and velocity maps of the simulated star with rotationnal flatenning and several other effects, which can be compared to interferometric observations.

2 SCIROCCO

2.1 Description of the Model

SCIROCCO stands for Simulation Code of Interferometric-observations for rotators and CirCumstellar Objects. It is written in `Matlab` and make use of the following semi-analytical approach, adopting the frame depicted in Fig. 1 (shown in cartesian reference): a pixellized intensity map is computed independently from a velocity map, and both are combined into a spectrally-resolved intensity image-cube, which can be input in a later step into an interferometric simulation code.

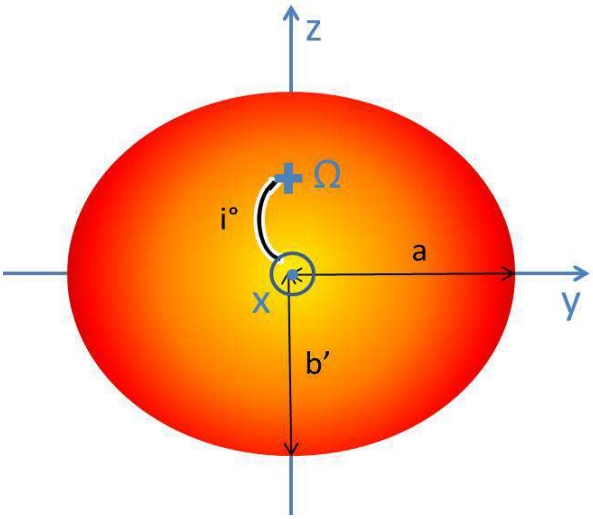

Fig. 1. Adopted reference system for a rotating star (flattened star with major axis a and minor axis b, here the apparent minor axis is $b' = ab/(a + (b - a)\cos i)$; assuming ellipsoid revolution principal/equations). The cross indicates the point where the rotation axis crosses the stellar surface. This rotation axis forms an angle i with the observer's direction (x axis) and its projection onto the sky is parallel to the z axis.

2.1.1 Intensity map

First, an intensity map of the star's photosphere is computed. We can use for example a simple limb-darkened model from (Hestroffer 1997), expressed in the geographical (co-latitude, longitude) coordinates (θ, ϕ):

$$I_c(\theta, \phi) = I_0(1 - \epsilon_\lambda(1 - \mu(\theta, \phi)) \tag{2.1}$$

where I_0 represents the flux at the center of the star, ϵ_λ is the limb darkening parameter, and $\mu(\theta, \phi)$ is the cosine of the angle between the normal to the surface at the point considered and the observer direction (Domiciano de Souza et al. 2004). The contour of the star is delimited by an ellipse with the minor axis in the direction of the rotation axis of the star. The minor-to-major axis depends on the rotation rate following the prescriptions of angle i (see Fig. 1). I_0 can serve as a weighting of the continuum flux as a function of wavelength (λ) using for example a Planck's law:

$$I_0(\lambda, T_{\rm eff}) = \frac{2hc^2}{\lambda^5} \frac{1}{e^{\frac{hc}{\lambda\sigma T_{\rm eff}}} - 1} \tag{2.2}$$

h being Planck's constant, c the speed of light, and $T_{\rm eff}$ the effective temperature of the star. I_0 can also be used to input the von Zeipel's effect into our model, by considering a co-latitude-dependent temperature in the below-mentioned local gravity field equation:

$$I_0(\theta) \propto F(\theta) = \sigma T_{\rm eff}^4(\theta) \tag{2.3}$$

with $T_{\rm eff}(\theta) \propto g^{0.25}(\theta)$, g being the local gravity field, also called the modulus of local effective surface gravity $g = \nabla\Psi(\theta)$, with $\Psi(\theta)$ is the stellar equipotential surfaces (Domiciano de Souza et al. 2004). An example of intensity map combining rotational flattening and gravity darkening is shown in Fig. 2 (left).

2.1.2 Velocity map

SCIRROCO produces a velocity map where for the moment, only rotation has been introduced:

$$V_{\rm proj}(\theta,\phi) = V_{\rm eq}\cos(\phi)(1-\alpha\sin^2(\theta))\sin(i) \tag{2.4}$$

In that equation, $V_{\rm eq}$ represent the equatorial rotation velocity, and the parameter α allows us to include a parametric differential rotation law (Domiciano de Souza et al. 2004). In the future, we also plan to include non-radial pulsations in that velocity map. An example of velocity map combining rotational flattening is shown in Fig. 2 (right).

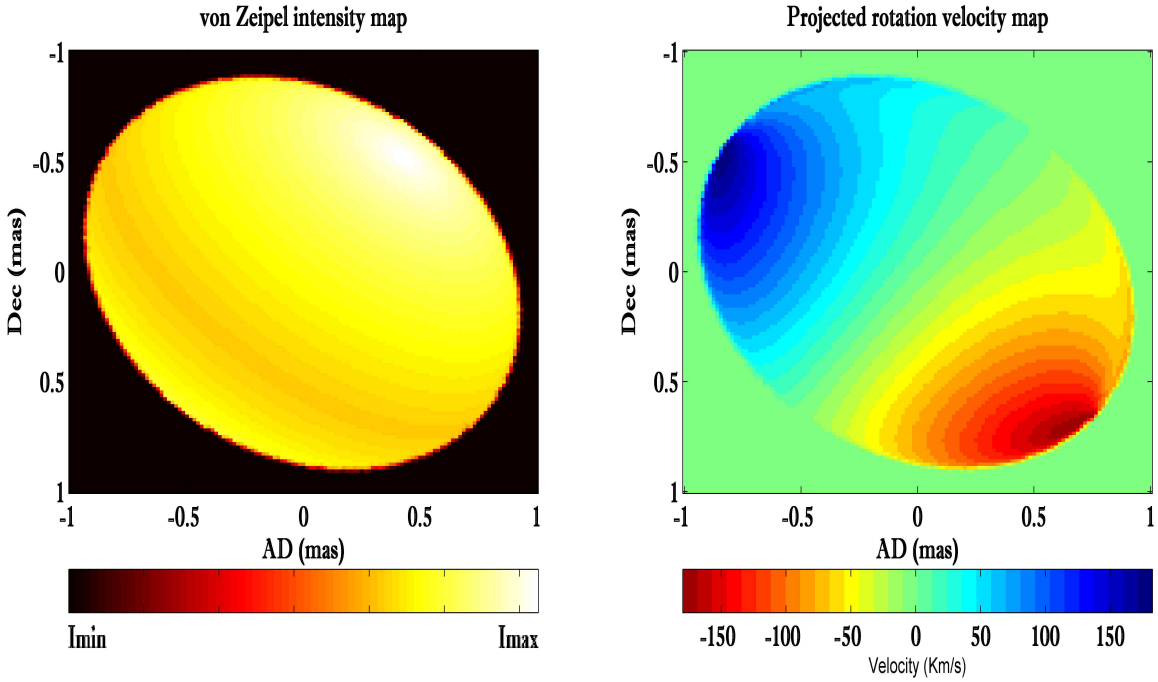

Fig. 2. Left: simulated Achernar intensity map in the continuum. The intensity at the poles is greater than at the equator. Here the velocity is around 88% of the critical velocity of the star. **Right:** velocity map of the same model (inclination 57°, orientation 39°). Here the simulated rotation is differential (the velocity of rotation at the equator is 60% larger than at the poles).

2.1.3 Spectrally-resolved image cube

The last step of the modelization process is to compute λ-dependent maps. For that, we need to model the natural line-profile of the considered line: we can assume e.g. Gaussian, Lorentzian, or Voigt profile:

$$\begin{cases} H_{\rm Gauss}(\lambda) = 1 - H_0 \left[-\pi H_0^2 \frac{(\lambda-\lambda_0)^2}{W^2} \right] \\ H_{\rm Lorentz}(\lambda) = 1 - \left[\frac{H_0}{1+(\frac{\lambda-\lambda_0}{W/2})^2} \right] \\ H_{\rm Voigt}(\lambda) = (H_{Gauss} * H_{Lorentz})(\lambda) \end{cases} \quad (2.5)$$

The last step calculates the intensity maps of the star as a function of wavelength. For that, we project via the Doppler effect the velocity map ($V_{\rm proj}$, Eq. 2.4) to the intensity map (I_c, Eq. 2.1), given the line profile (H, Eq. 2.5) and the work wavelength λ:

$$I(\lambda, \theta, \phi) = H \left(\lambda + \lambda_0 \frac{V_{\rm proj}(\theta, \phi)}{c} \right) I_c(\theta, \phi) \quad (2.6)$$

We get one intensity map per wavelength of interest around the central wavelength λ_0 of the line (see Fig. 3, left). Once all intensity maps are computed, we synthesize the interferometric observables by Fourier-Transforming each map (see Fig. 3, right). This provide us spectra, visibility amplitudes, phases, and closure phases.

By comparing the observed interferometric measurements to the synthesized quantities, we can access to the parameters of the fast rotating star such as: effective temperature as a function of co-latitude, rotational rate, inclination, angular radius and flattening and, if possible the differential rotation.

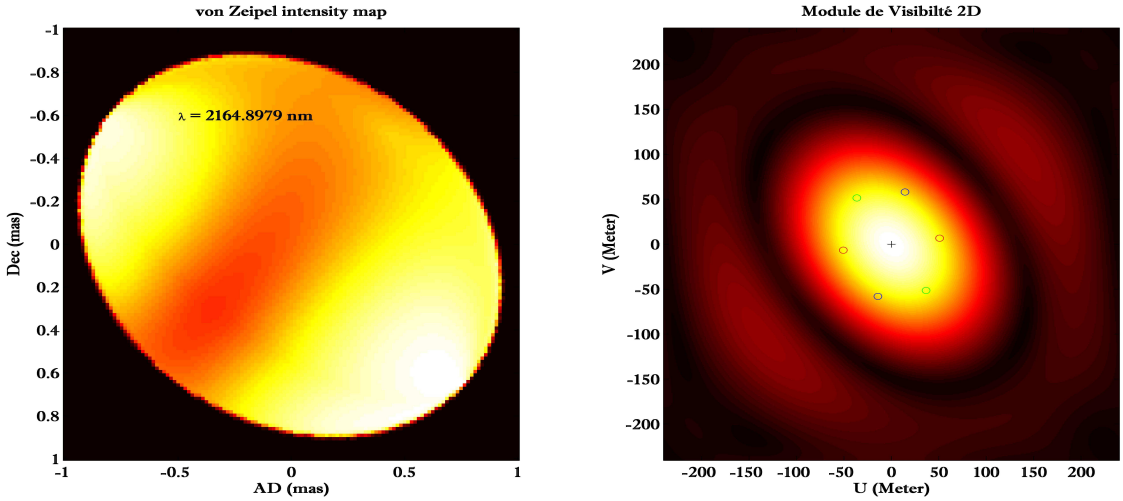

Fig. 3. Left: monochromatic intensity map for a given wavelength. **Right:** Map of corresponding 2D module visibility, which is represented on the three bases with interferometric which will make the observation (1st base small red circle, 2nd green and 3rd blue).

2.2 Simulation of interferometric observations: the example of Achernar

To illustrate this paper, we simulate the famous Be star Achernar with SCIROCCO as observed in Domiciano de Souza et al. (2003). We use the parameters detailed in the paper, which are recalled for practicity in Table 1.

Table 1. Achernar parameters (from Domiciano de Souza et al. 2003)

Star	*Achernar (α Eri)*	*v/v_{crit}*	*0.79-0.96*	**T_{eq} (K)**	*9500-14800*
Spectral type	*B3Vpe*	**Orientation (°)**	*39±1*	**R_{pole} ($R\odot$)**	*8.3-9.5*
Velocity v (km/s)	*225*	**Gravity darkening β**	*0.25*	**R_{eq} ($R\odot$)**	*12.0±0.4*
Inclination i (°)	*57*	**T_{pole} (K)**	*20000*	**Oblateness**	*0.348±0.10*

In addition, we introduce to our model a differential rotation coefficient ($\alpha = 0.6$) and a Voigt intrinsic line profile with a depth of 0.6 and a $FWHM = 10 * \Delta\lambda$.

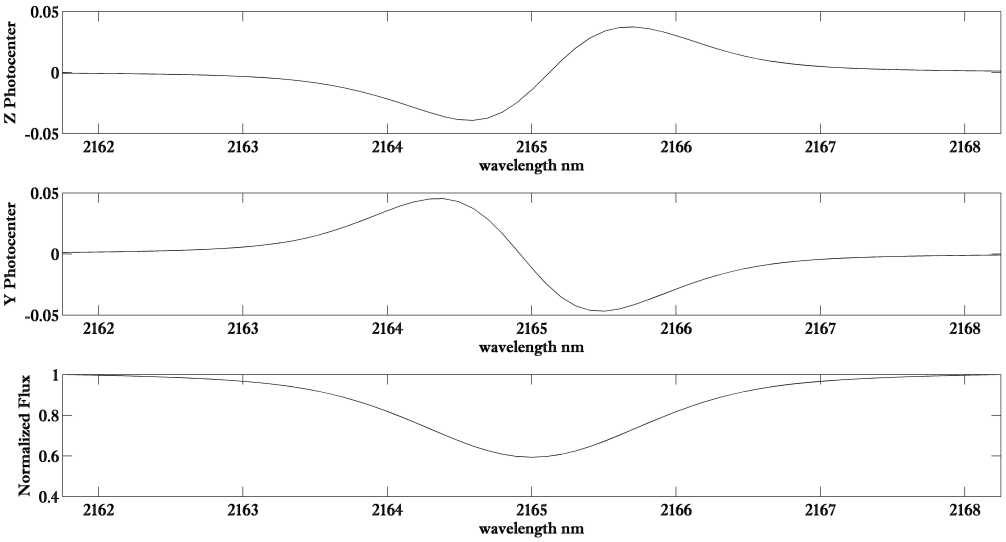

Fig. 4. Top: photo-center (or centroid: the first order term of the phase by Mac Lauren development, Jankov et al. (2001)) along the Z axis (see reference adopted Fig.1). **Middle:** photo-center by Y (note that the photo-centers are in radian). **Bottom:** normalized spectrum, we see well that our starting line has expanded and its depth was decreased (precisely because of the rotation).

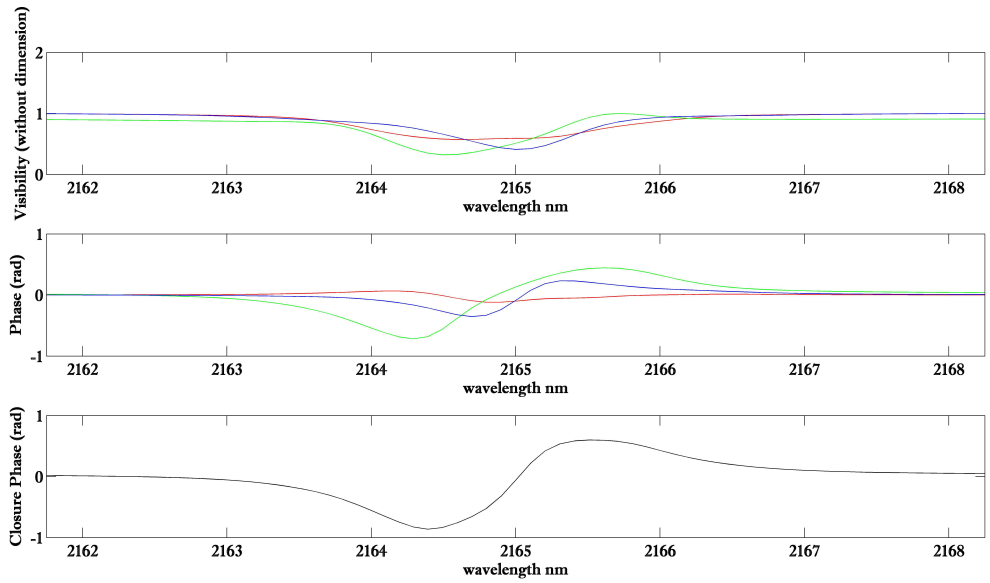

Fig. 5. Top: visibility module observed by the interferometric three bases (red, green and blue). **Middle:** the phases observed in the three interferometric bases (red, green and blue), we note that although the phase observed by the base perpendicular to the axis of rotation of the star (green) is the one that has the highest amplitude & inversely that which is along the axis of rotation (red) is the lowest. **Bottom:** the closure phase.

We choose to simulate interferometric observations with the AMBER/VLTI instrument on the 3 following interferometric baselines : G1-D0 (51.28 m, $-82.5°$), D0-H0 (63.12 m, $35.42°$), H0-G1 (59.78 m, $-13.8°$), and around the Brackett γ line (2.165μ m).

The velocity map & intensity map in the continuum continuum are shown in Fig. 2, the monochromatic intensity map at a given wavelength & corresponding 2D visibility amplitude map in Fig. 3, the photo-centers

& spectrum in Fig. 4, and finally visibilities, phases & closure phase in Fig. 5.

3 Conclusions & Discussions

We presented here a semi-analytical model of fast-rotators whose aim is to interpret interferometric datasets. We are able to produce interferometric observables using a set of physical parameters like the rotation law, gravity darkening effect, etc., while keeping the computing time reasonable (one set of visibility curves can be computed in $15s$).

The next step is to develop a "model-fitting" approach to compare real datasets with this model.

References

Chelli A., & Petrov R.G. 1995, A&A, 109, 401
Collins, G. W. 1974, ApJ, 191, 157
Collins, G. W., & Harrington J. P. 1966, ApJ, 146, 152
Collins, G. W., & Sonneborn, G. H. 1977, ApJ, 34, 41
Domiciano de Souza, A., Zorec, J., Jankov, S., Vakili, F., Abe, L. 2004, A&A 418, 781
Domiciano de Souza, A., Kervella, P., Jankov, S., Abe, L., Vakili, F. et al. 2003, A&A, 407, L47
Domiciano de Souza, A., Vakili, F., Jankov, S., Janot-Pacheco, E. & Abe, L. 2002, A&A, 393, 345
Hestroffer, D. 1997, A&A, 327, 199
Hutchings, J. B., & Stoeckley, T. R. 1977, PASP, 89, 19
Hutchings, J. B., Nemec, J. M., & Cassidy, J. 1979, PASP, 91, 313
Jankov, S., Vakili, F., Domiciano de Souza, A., & Janot-Pacheco, E. 2001, A&A, 377, 721
Maeder, A., & Peytremann, E. 1972, A&A, 21, 279
Martayan, C., Frémat, Y., Hubert, A.-M., Floquet M., Zorec J. et al. 2006, A&A, 452, 273
Meynet, G. 2009, Lecture Notes in Physics, 765, 139
van Belle, G. T. 2012, A&ARv, 20, 51
von Zeipel, H., 1924, MNRAS, 84, 665